Path-integral study of a two-dimensional Lennard-Jones glass

P. Ballone[1] and B. Montanari[2]

[1]*Dipartimento di Fisica and Istituto Nazionale di Fisica della Materia, Università di Messina, Contrada Papardo, 98166 Messina, Italy*

[2]*Department of Chemistry, Imperial College of Science Technology and Medicine, South Kensington, London SW7 2AY, United Kingdom*

(Received 14 December 2001; revised manuscript received 11 April 2002; published 20 June 2002)

The glass transition in a quantum Lennard-Jones mixture is investigated by constant-volume path-integral simulations. Particles are assumed to be distinguishable, and the strength of quantum effects is varied by changing $\hbar$ from zero (the classical case) to one (corresponding to a highly quantum-mechanical regime). Quantum delocalization and zero point energy drastically reduce the sensitivity of structural and thermodynamic properties to the glass transition. Nevertheless, the glass transition temperature T_g can be determined by analyzing the phase space mobility of path-integral centroids. At constant volume, the T_g of the simulated model increases monotonically with increasing $\hbar$. Low temperature tunneling centers are identified, and the quantum versus thermal character of each center is analyzed. The relation between these centers and soft quasilocalized harmonic vibrations is investigated. Periodic minimizations of the potential energy with respect to the positions of the particles are performed to determine the inherent structure of classical and quantum glassy samples. The geometries corresponding to these energy minima are found to be qualitatively similar in all cases. Systematic comparisons for ordered and disordered structures, harmonic and anharmonic dynamics, classical and quantum systems show that disorder, anharmonicity, and quantum effects are closely interlinked.

DOI: 10.1103/PhysRevE.65.066704 PACS number(s): 64.70.Pf, 05.30.−d, 66.35.+a, 63.20.Pw

I. INTRODUCTION

Computer simulation nowadays plays an ever increasing role in the investigation of simple glasses, partly because the recent, astonishing surge of computer power has dramatically expanded the reach of simulation methods, and, more importantly, because new ideas and paradigms are emerging from the concerted effort of several computational groups [1,2]. In recent years the discussion has been focused on two major topics: (i) the nature of the glass transition [3]; (ii) the investigation of the low-energy excitation typical of glasses [4], i.e., the soft quasilocalized modes giving rise to the Boson peak at ~ 10 K, and the two-level systems responsible for the linear term in the specific heat at ~ 1 K [5]. Atomistic simulations, in particular, have helped in the identification of the structural features associated with those low-energy excitations: low frequency quasilocalized vibrational states have been identified and characterized in several studies [6], and their role in the glass transition has been investigated [7]. In most of these studies, often based on idealized interatomic potentials (Lennard-Jones or repulsive soft spheres), an amorphous sample is prepared by quenching a liquid system by classical molecular dynamics (MD) or Monte Carlo (MC) simulation. Two approaches have been used to analyze the dynamical properties of the resulting amorphous system: (i) the computation and diagonalization of the dynamical matrix and (ii) the analysis of trajectories generated by classical MD at low temperature. Quantum-mechanical effects are easily accounted for by the first method, and soft quasilocalized states can be identified by their low frequency and limited spatial extension. This approach, however, is limited to harmonic properties, although anharmonic contributions can be partially included by a variant of this method (i.e., the quasiharmonic approximation). On the other hand, classical MD treats harmonic and anharmonic effects on the same footing. The drawback of this method is that, at low temperature, the time evolution generated by Newton's equations of motion does not correspond to the true system dynamics, and therefore MD should be considered simply as a way to explore the potential energy landscape visited by the amorphous system. Tunneling modes can be identified by observing the thermal activated oscillations of the system between two or more quasidegenerate configurations. In previous studies based on this method, quantum tunneling has been investigated *a posteriori*, either by a semiclassical WKB analysis of the potential energy profile connecting the minima identified in the simulation [8,9], or using phenomenological models for the double well potential giving rise to the two-level system, and fitted to simulation results for two-dimensional (2D) [10] and 3D [11] samples.

The self-consistent inclusion of anharmonicity and quantum effects in models of amorphous solids at low temperature would provide a more complete and realistic description of these systems, and could reveal new and unexpected features. As a first step towards this goal, we perform a path-integral (PI) simulation of a model Lennard-Jones glass in 2D. The particles are assumed to be distinguishable and of equal mass, and the strength of quantum effects is measured by the value of Planck's constant $\hbar$, which is varied from zero (the classical limit) to one (corresponding to a highly quantum-mechanical regime, as it will be apparent from the results discussed in the following sections [12]).

We restrict ourselves to two-dimensional systems because the results for the quasilocalized tunneling modes and for the system configurations are easier to analyze and to display in graphical form. In analogy with what is done in classical MD, we prepare the system in the liquid state, and progressively quench it down to very low temperature. As described in detail below, most of our computations concern a binary mixture that is known to remain homogeneous and disordered under all annealing cycles achievable by computer simulation.

The computational results provide a solid ground to address three problems: (i) the characterization of the glass transition in a quantum-mechanical system; (ii) the comparison of the amorphous structure for classical and quantum-mechanical systems evolving under the same Hamiltonian; (iii) the identification and characterization of low-energy excitations.

The identification of the glass transition by MD simulations, and the appropriate comparison with experimental measurements, is still the subject of active investigation even in the case of classical systems. The standard definition adopted in experiments (the glass transition is where the viscosity coefficient reaches 10^{13} P) cannot be extended to computer experiments because the evaluation of such a high viscosity would require exceedingly long simulation times [13]. Alternative criteria have been proposed, based on either thermodynamic properties (the appearance of broad specific heat anomalies) or structural properties (the splitting of the second neighbors' peak in the radial distribution function, and the growth of a prepeak in the structure factor).

In quantum-mechanical simulations, all these criteria lose (partially or entirely) their ability to identify the glass transition. In the first instance, the imaginary-time formulation of most computational approaches for quantum systems hinders the determination of dynamical properties such as diffusion or viscosity. In addition, quantum delocalization and zero point energy conceal the typical signatures of the glass transition, which otherwise appear in the structural and thermodynamic properties. Despite these difficulties, it is nevertheless possible to determine the glass transition temperature T_g of quantum systems by a detailed analysis of the mobility of quantum paths (more precisely, of quantum paths' centroids) in phase space. The characteristic regimes of liquidlike mobility at high temperature, activated discrete jumps at intermediate temperature, and solidlike glassy behavior at low T, are still recognizable in the behavior of quantum systems, although quantitative estimates for the diffusion coefficient cannot be obtained. This separation of dynamical regimes (that remains unaltered over a wide range of simulation time scales) provides the most effective approach for identifying the glass transition.

For our glasses, although the classical and quantum-mechanical trajectories of the particles differ, the underlying potential energy valleys are, to a large extent, equivalent. This becomes evident when we quench various configurations, selected from either classical or quantum trajectories, and analyze the average structural properties (such as the radial distribution function or the structure factor) of the static geometries corresponding to the potential energy minima [14]. We find that these average structural properties are practically indistinguishable in all cases, whereas the same functions computed at nonzero temperature during classical and quantum simulations are, as expected, markedly different.

A similar analysis of potential energy minima is used to identify tunneling centers, and to investigate the interplay of quantum and thermal effects on their dynamics. It is worth pointing out that the tunneling modes themselves are characterized by low excitation energies, and therefore they are expected to behave classically at all but the lowest temperatures. However, their interaction with a classical or a quantum-mechanical thermal bath may be different, and it is precisely this difference that is investigated in our study.

The interest in this kind of problems, and in our 2D study in particular, is enhanced by the experimental preparation of quenched noble gas films on a cold substrate [15], at temperatures (a fraction of a °K) such that quantum-mechanical effects are expected to play a significant role.

II. THE MODEL AND THE COMPUTATIONAL METHOD

We study a binary mixture of particles interacting via a Lennard-Jones (LJ) potential

$$v_{i,j}(r)=4\epsilon_{ij}\left[\left(\frac{\sigma_{ij}}{r}\right)^{12}-\left(\frac{\sigma_{ij}}{r}\right)^{6}\right], \tag{1}$$

where the indexes i,j refer to the particle species (1 and 2), which differ for the LJ diameter only: $\sigma_{22}=1.5\sigma_{11}$, with $\sigma_{12}=(\sigma_{11}+\sigma_{22})/2$ [16]. All the other parameters (i.e., ϵ_{ij} and the particle mass M) are the same for the two species. Reduced units are used throughout the paper by setting $\sigma_{11}=1$, $\epsilon_{11}=1$, and $M=1$. This implicitly defines our unit of time as $\tau=\sigma_{11}\sqrt{M/\epsilon_{11}}$.

We consider a system of $N=N_1+N_2=1000$ particles, with number concentrations $x_1=N_1/N=0.8$, and $x_2=N_2/N=0.2$. Two-dimensional periodic boundary conditions are applied, assuming a square unit cell of side L. Previous studies have shown that systems with this Hamiltonian and composition do not crystallize during classical MD simulations of ordinary length (see, for instance, Ref. [17] and Ref. [18]). All computations are done for systems whose density $\rho=N/L^2=0.952$ is equal to the density of the systems investigated in Ref. [17]. In 2D, the size ($N=1000$) of our samples enables us to explore the intermediate range order (beyond the third nearest neighbors' shell) with little influence of finite size effects, and at the same time it allows extensive simulations with the PI method.

The path-integral simulation is performed by exploiting the well known isomorphism of the quantum trace operation with the phase space integration for a classical system of N cyclic polymers of length P, moving on the potential energy surface [19–21],

$$\begin{aligned}V(\mathbf{r_{1,1}},\ldots,\mathbf{r_{1,P}};\ldots;\mathbf{r_{N,1}},\ldots,\mathbf{r_{N,P}}) \\ =\sum_{i=1}^{N}\sum_{j=1}^{P}\Bigg(\alpha(T)(\mathbf{r_{i,j}}-\mathbf{r_{i,j+1}})^2 \\ +\frac{1}{P}\sum_{k=1}^{N}v_{i,k}(|\mathbf{r_{i,j}}-\mathbf{r_{k,j}}|)\Bigg),\end{aligned} \tag{2}$$

with $\mathbf{r_{i,P+1}}=\mathbf{r_{i,1}}$ and

$$\alpha(T)=\frac{PM}{2\hbar^2\beta^2}. \tag{3}$$

In these equations, P is the order of the path-integral discretization in imaginary time, $\beta = 1/k_B T$ is the inverse temperature in energy units (k_B is Boltzmann's constant), and $\hbar$ is used here as a free parameter measuring the strength of quantum effects. The set of coordinates $\{\mathbf{r}_{k,j}, k=1,N\}$, at fixed j, represents the system configuration at the imaginary time $\tilde{t} = i(\beta j/P)$. Following standard naming conventions, this set of coordinates is also named an *imaginary-time slice*, while the position $\mathbf{r}_{k,j}$ of particle k at the imaginary-time slice j identifies a *bead*. We limit ourselves to this so-called *primitive algorithm* because of its simplicity, and because, despite its relatively low efficiency, we could simulate all conditions of interest for our study with an affordable computational effort.

We sample the phase space of this system by MD [22] in the microcanonical ensemble by using the velocity Verlet algorithm [23]. The mass of the beads is set to M/P, in such a way that the total mass of each polymer representing one particle is always equal to one.

The discretization of the path integrals is performed with the constraint

$$\frac{PM}{\hbar^2 \beta} = 72. \tag{4}$$

We verify that this choice, which fixes the temperature dependence of P, provides a reasonably well converged representation of the total energy [24], while, at the same time, it is not so large to cause severe ergodicity problems [20]. In particular, we verify that external perturbations applied to selected degrees of freedom are equilibrated well within 10^4 MD steps, i.e., a time much shorter than the length of our runs (all beyond 3×10^5 steps). The relatively stiff harmonic potential in Eq. [2], however, limits the value of our time step to $\delta t = 1.2\times 10^{-3}\tau$. This is the time step used in all our simulations, including the classical ones. Each system is simulated at values of temperature in the interval $1 \leqslant T \leqslant 12$ and corresponding to integer P values.

The quantum-mechanical average total energy is evaluated as detailed in Ref. [25]. The kinetic energy E_K, in particular, is evaluated using the virial estimator [26,27],

$$E_K = \frac{3N}{2\beta} + \frac{1}{2P} \times \left\langle \sum_{i=1}^{N} \sum_{j=1}^{P} \frac{\partial \sum_{k=1}^{N} v_{i,k}(|\mathbf{r}_{\mathbf{i},\mathbf{j}} - \mathbf{r}_{\mathbf{k},\mathbf{j}}|)}{\partial \mathbf{r}_{\mathbf{i},\mathbf{j}}} \cdot (\mathbf{r}_{\mathbf{i},\mathbf{p}} - \mathbf{r}_{\mathbf{k},\mathbf{p}}) \right\rangle, \tag{5}$$

which is known to be the least affected by fluctuations among all simple estimators that can be derived from the partition function of the system.

The usage of MD to compute quantum-mechanical properties is justified only if the simulation temperature T_{MD}, defined by the average kinetic energy along the MD trajectory, is close to the temperature T entering the definition of the coupling parameter $\alpha(T)$ [see Eq. (3)]. In each of our runs, the relative difference between T and T_{MD} is always smaller than 1%. However, we noticed that several average quantities (such as the quantum-mechanical kinetic and potential energy, the imaginary-time correlation functions, etc.) are very sensitive to even small deviations of T_{MD} from T. For this reason, we numerically compute the derivative of each quantum-mechanical average with respect to T_{MD} at fixed $\alpha(T)$ and P, and correct the simulation results by linearly extrapolating to $T_{MD} = T$.

As mentioned in the introduction, in order to discriminate between harmonic and anharmonic effects, we analyze the vibrational properties of our systems in the harmonic approximation. To this aim, local minima of the system potential energy are found by quenched MD [28]. Then, the second derivatives of the energy with respect to the particle positions are computed by a finite differences scheme, and the corresponding dynamical matrix is diagonalized to provide vibrational eigenvalues and eigenstates. At the density of our simulations ($\rho = 0.952$), the particles mainly sample the repulsive part of the LJ potential, giving rise to stiff vibrational modes that, in turn, greatly enhance the strength of quantum effects.

The interpretation of our simulation results concerning anharmonic dynamics is eased by considering the so-called centroid molecular dynamics (CMD, introduced in Ref. [29] and reviewed in Ref. [30]), although we did not use this method in our study. In the CMD approach, the basic variables are the centroids $\{\mathbf{R}_\mathbf{i}^\mathbf{C}, i=1,N\}$ of the paths representing each particle,

$$\mathbf{R}_\mathbf{i}^\mathbf{C} = \frac{1}{P} \sum_{j=1}^{P} \mathbf{r}_{\mathbf{i},\mathbf{j}}, \tag{6}$$

together with the corresponding conjugate momenta $\{\mathbf{Q}_\mathbf{i}^\mathbf{C}, i = 1,N\}$. An approximate and yet reliable formulation for the time evolution of these variables is

$$\dot{\mathbf{R}}_\mathbf{i}^\mathbf{C} = \frac{\mathbf{Q}_\mathbf{i}^\mathbf{C}}{M}, \tag{7}$$

$$\dot{\mathbf{Q}}_\mathbf{i}^\mathbf{C} = \mathbf{F}_\mathbf{i}^\mathbf{C}, \tag{8}$$

where $\mathbf{F}_\mathbf{i}^\mathbf{C}$ is the force on the particle i averaged on all paths whose centroid is fixed at $\mathbf{R}_\mathbf{i}^\mathbf{C}$. In the CMD framework, the expression for the diffusion coefficient involves only the position vectors of the centroids,

$$D = \frac{1}{2dN} \lim_{t\to\infty} \frac{1}{t} \sum_{i=1}^{N} \langle |\mathbf{R}_\mathbf{i}^\mathbf{C}(t+t_0) - \mathbf{R}_\mathbf{i}^\mathbf{C}(t_0)|^2 \rangle, \tag{9}$$

where d is the dimensionality of the system and the average is over different initial times t_0. This simple quantum-classical correspondence is due to the fact that diffusion is related to the zero-frequency limit of dynamical correlation functions, and behaves classically provided that quantum fluctuations are accounted for in the computation of the forces (see Ref. [30] for more details). These formal relations are supported by explicit simulation results showing that classical and quantum systems evolving on the same potential energy surface have a quantitatively different but qualitatively similar diffusion behavior.

One can think of the centroid trajectories generated in our PI-MD simulations as intermediate between those computed in CMD and the classical ones. On the one hand, since each bead has mass M/P, it is easy to verify that along our trajectories the centroid coordinates and momenta satisfy the equations

$$\dot{\mathbf{R}}_{\mathbf{i}}^{\mathbf{C}}=\frac{\mathbf{Q}_{\mathbf{i}}^{\mathbf{C}}}{M} \tag{10}$$

and

$$\dot{\mathbf{Q}}_{\mathbf{i}}^{\mathbf{C}}=\frac{1}{P}\sum_{j=1}^{P}\sum_{k\neq i}^{N}\frac{\partial v_{i,k}(|\mathbf{r}_{\mathbf{i},\mathbf{j}}-r_{k,j}|)}{\partial \mathbf{r}_{\mathbf{i},\mathbf{j}}}, \tag{11}$$

and, therefore, the force driving the evolution of $\dot{\mathbf{Q}}_{\mathbf{i}}^{\mathbf{C}}$ in our simulations is not equal to $\mathbf{F}_{\mathbf{i}}^{\mathbf{C}}$.

On the other hand, because the ratio between the mass of the centroids and that of the beads is $P \gg 1$, the time evolution of our samples consists of rapid fluctuations in the discrete paths superimposed to the slow motion of the centroids. These rapid fluctuations provide at least part of the force averaging implied in the definition of the $\mathbf{F}_{\mathbf{i}}^{\mathbf{C}}$'s, although an exact correspondence between $\dot{\mathbf{Q}}_{\mathbf{i}}^{\mathbf{C}}$ and $\mathbf{F}_{\mathbf{i}}^{\mathbf{C}}$ is obtained only in the $P\rightarrow\infty$ limit.

This argument, which relies on the same adiabatic principle exploited by other simulation techniques [31], is used in Sec. IV to discuss qualitatively the diffusive behavior of our systems in terms of the centroid trajectories given by our PI-MD simulations. In particular, we shall distinguish three different regimes: (i) a high temperature range, in which centroids move continuously in a liquidlike fashion; (ii) an intermediate regime, in which centroids perform discrete jumps that result in a slow diffusion of the system in phase space; (iii) a low temperature range, in which centroids are localized in space, sometimes oscillating among nearly degenerate and spatially contiguous potential energy minima. We emphasize that, even for very large values of P, the approximate relation between $\dot{\mathbf{Q}}_{\mathbf{i}}^{\mathbf{C}}$ and $\mathbf{F}_{\mathbf{i}}^{\mathbf{C}}$ underlying our analysis does not imply that our path-integral dynamics approaches the true dynamics, since, in the CMD method, simulation time is not equivalent to real time. An approximate correspondence (correct up to order $\hbar^2$) can be established only for harmonic modes, and the rescaling factor connecting simulation time to real time depends explicitly on the frequency of the mode to which it is applied [30]. For this reason, no quantitative estimate of the diffusion coefficient is obtained from our PI-MD simulations.

In order to analyze the interplay of temperature, quantum effects and disorder on the behavior of our system, we study a sequence of systems of increasing quantum-mechanical character, obtained by progressively switching $\hbar$ on. In the units specified above, we consider $\hbar^2=1/3$, 1/2, and 1 (equivalently, we could think of systems with decreasing particle mass and studied at constant value of $\hbar$ [32]). To provide a comparison for the quantum-mechanical study, we first perform a classical MD simulation, corresponding to $\hbar^2=0$, whose results are discussed in the following section. The results of additional computations done for $\hbar^2=1/6$ and 1/4 display the same qualitative features of simulations at higher $\hbar^2$, and therefore they are not discussed in detail here. All these values of $\hbar^2$ correspond to highly quantum-mechanical systems, as will be apparent from the results reported below. An independent measure of the strength of quantum-mechanical effects is provided by the dimensionless de Boer parameter $\Lambda=\hbar/\sigma\sqrt{M\epsilon}$ that, for instance for rare gas atoms, assumes values from $\Lambda=0.427$ for He to $\Lambda=0.01$ for Xe. In our simulations, this parameters varies from $\Lambda=1$ for $\hbar^2=1$ to $\Lambda=0.41$ for $\hbar^2=1/6$. However, because we use $\hbar$ as an independent variable and we choose M, σ, and ϵ as basic units, our simulations do not correspond exactly to any real rare gas system at the physical value of $\hbar$.

III. CLASSICAL SIMULATION

Our simulations for the classical case are similar to those reported in Ref. [17], and consist of a MD quench from the fluid to the glass phase. Our equilibration and statistics runs are shorter than those of Ref. [17], for consistency with the quantum-mechanical computations, which are computationally more expensive.

A liquid sample is equilibrated at $T=6$ during 2×10^6 time steps (corresponding to 2400τ), statistics is accumulated over a second run of equal length and then the system kinetic energy is discontinuously reduced by an amount corresponding to $\Delta T=0.25$. A similar equilibration/quench sequence is repeated several times, until the system reaches $T=0.5$.

Inspection of snapshots for the low temperature structure shows that the system is in a clearly recognizable microcrystalline state, with the majority component (type 1 particles) forming crystallized grains delimited by elongated islands of type 2 particles (see Fig. 1). Disorder arises at the boundary of the two components and disrupts the long range translational and orientational order.

The internal energy U (averaged over the statistics runs of 2400τ) is an almost linear function of T. To emphasize nonlinear contributions, we fit the low temperature region of $U(T)$ $(T<1.5)$ with a linear function $[U_{lin}(T)=a+bT]$, and we report the difference $U(T)-U_{lin}(T)$ in Fig. 2(a). The potential energy contribution C_v^U to the constant volume specific heat is computed by projecting $U(T)$ on orthogonal polynomials, and then differentiating the polynomial fit with respect to T. The results are shown in Fig. 2(b). Both $U(T)-U_{lin}(T)$ and $C_v^U(T)$ display a broad anomaly in the temperature range $2<T<4$. The analysis of MD trajectories at several temperatures allows us to relate this anomaly to the heat release due to the formation of crystalline islands of type 1 particles. In other words, the transition displayed by the model has a weak first order character, due to the partial freezing of type 1 particles, limited by the presence of the minority (type 2) particles. In this respect, the results for $U(T)$ and for $C_v^U(T)$ are somewhat different from the stan-

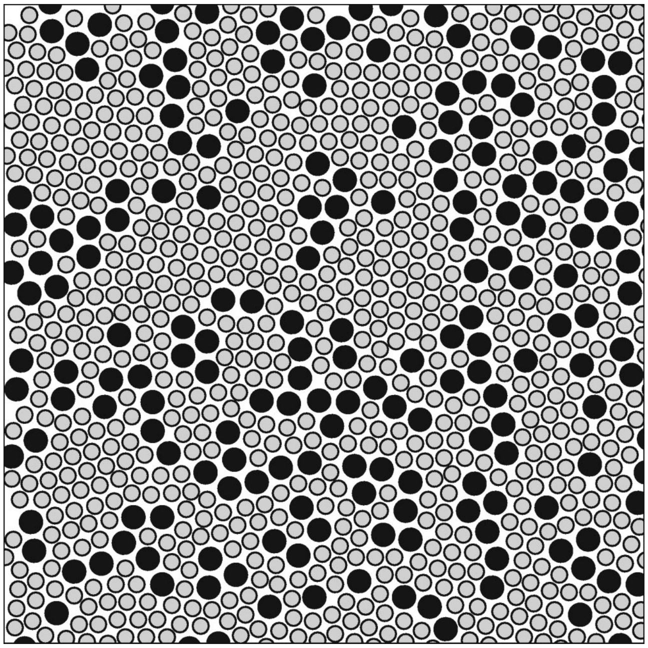

FIG. 1. Typical low temperature configuration found in the classical simulation. Gray and black circles represent the particles of type 1 and 2, respectively.

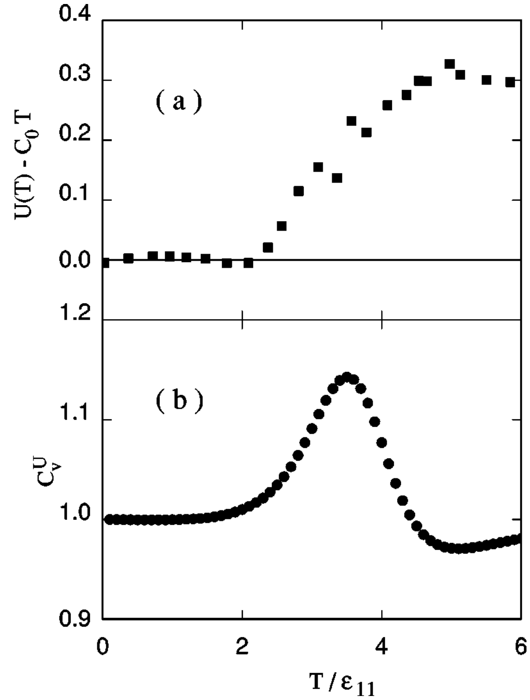

FIG. 2. Thermodynamic properties of the classical ($\hbar=0$) model. (a) Average potential energy per particle U as a function of temperature T. A linear term has been subtracted to emphasize nonlinear contributions. (b) Potential energy contribution to the constant volume specific heat as a function of T.

dard picture of the glass transition, in which the specific heat changes abruptly but continuously from a low value below T_g to a high value above T_g (see, for instance, Fig. 1 in Ref. [1]).

The diffusion coefficient, as a function of T, computed in our simulations agrees well with the one reported in Ref. [17], thus confirming that our shorter runs are nonetheless sufficient to describe the system behavior at a satisfactory level of accuracy. The analysis of trajectories shows that, as expected, the smaller particles (type 1) diffuse systematically faster than the larger ones. The qualitative behavior of $|r_i(t)-r_i(0)|^2$ (where i is a generic particle in the system), however, is similar for the two species. For $T>3$, for instance, $|r_i(t)-r_i(0)|^2$ displays a smooth and nearly monotonic dependence upon time, whereas for $2\leq T\leq 3$ diffusion takes place by discontinuous, thermally activated jumps. During our standard runs (extending over 2400τ) no diffusion is detected for either species for $T\leq 1.75$. Longer runs ($\sim 12\,000\tau$) at $T=1.5$ revealed a handful of localized jumps, that, however, do not appear to give rise to connected trajectories extending over long distances. These observations allow us to locate the glass transition temperature at $T_g=2$. This estimate of T_g depends on the time scale of our MD *observations* and could, in principle, change slightly towards lower temperatures by considering much longer MD runs. However, we verified that the dependence of T_g on the observation time scale is relatively weak. For instance, quenching the system at twice the cooling rate does not change the results for $U(T)$ significantly for both the low T structure and the temperature dependence of the diffusion coefficient, thus leaving our estimate for T_g also unchanged.

Our identification of T_g is supported by the analysis of the radial distribution function and structure factor. The radial distribution function, for instance, progressively develops the typical features often associated with amorphous systems (a split second peak and a succession of less well defined oscillations at intermediate distances) over the range $2\leq T\leq 3$. These features are only slightly enhanced by decreasing the temperature to $T=1.75$, and remain nearly unchanged upon quenching to lower temperatures.

As a further comparison for our PI results, we carry out classical simulations for an *average* monocomponent system with the same number of particles N, and with a LJ diameter σ defined by

$$N\sigma^2=N_1\sigma_1^2+N_2\sigma_2^2.$$

This choice fixes the area covered by the particles of the monocomponent system to be equal to that of the binary mixture [33]. On cooling this system from high T we observe, as expected, a clear first order crystallization transition at $T=9.3$. The large difference between this temperature and T_g of the two-component system is a measure of the drastic disruption of long range order and low T mobility, due to the size asymmetry between type 1 and type 2 particles.

In order to further analyze the effects of disorder we first perform a careful optimization of the low T structure of both the mixture and the *average* monocomponent system by quenched MD [28], so as to minimize the potential energy. Subsequently, we determine the harmonic vibrational properties via the method briefly described in Sec. II. The comparison of the results for the mixture and the crystalline monocomponent system shows that, as expected, the disor-

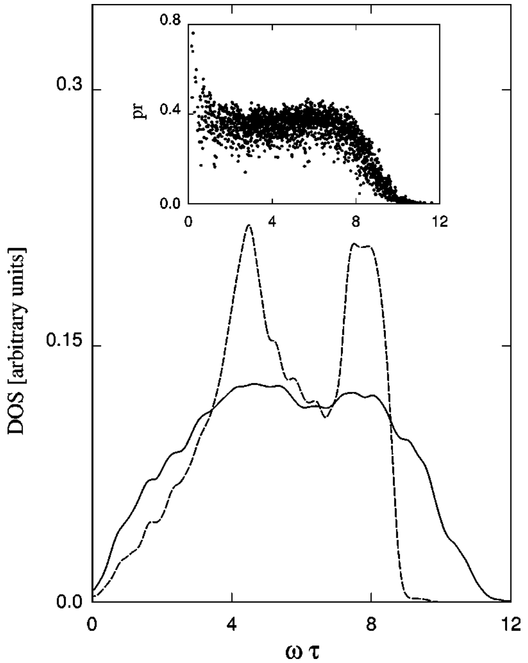

FIG. 3. Vibrational density of states from harmonic analysis for the classical case. Full line, two component glassy mixture; dashed line, crystalline monocomponent system with same packing as the mixture (see Sec. III). Inset: participation ratio pr for each harmonic mode (small values of pr identify localized modes).

dered mixture displays an excess density of states at low frequency, and a long tail at high energy (see Fig. 3). The participation ratio pr, which measures the number of particles involved in each of the harmonic modes [34], shows that this high energy tail is due to highly localized modes (see the inset of Fig. 3). Furthermore, a few of the low energy modes are localized ($pr<0.2$) [35]. The analysis of the corresponding eigenvectors shows that these modes concern compact clusters of particles at the interface between type 1 grains and type 2 particles. For these modes, only the particles of type 1 move significantly. The relation between these localized soft modes and quantum-mechanical tunneling centers will be discussed in Sec. VII.

IV. THE GLASS TRANSITION IN THE QUANTUM-MECHANICAL MODEL

The identification of the glass transition for the quantum-mechanical model represents a major challenge for our PI simulations since, as $\hbar$ increases, thermodynamic, structural, and dynamical properties become either too insensitive to T, or too difficult to compute quantitatively, hence making the determination of T_g far more problematic than in the classical case.

The most effective criterion that we found for our investigation is based on the analysis of the diffusive behavior of the particle centroids, and relies on the approximate classical-quantum correspondence discussed in Sec. II. Because of computational convenience, we do not discuss the diffusion coefficient directly, instead we use a closely related quantity, called the Lindemann index, defined as

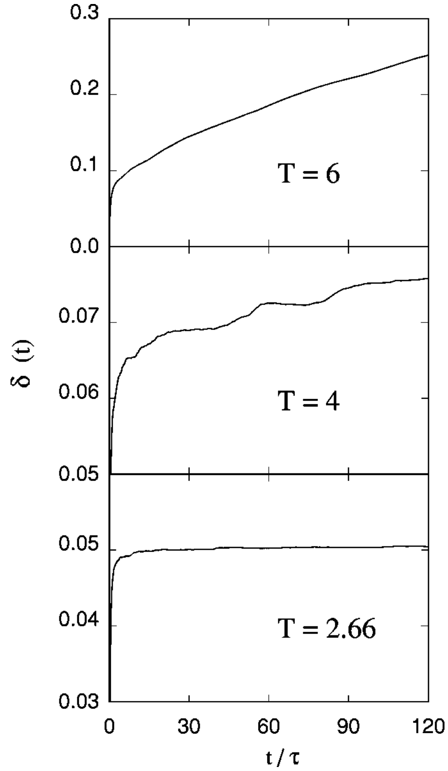

FIG. 4. Time-dependent Lindemann index δ as a function of averaging time t for three temperatures and $\hbar^2=1$.

$$\delta=\frac{1}{N_p}\sum_{i<j}\frac{\sqrt{\langle R_{ij}^2\rangle-\langle R_{ij}\rangle^2}}{\langle R_{ij}\rangle}, \tag{12}$$

where R_{ij} is the distance between the centroids for particles i and j, and N_p is the number of pairs included in the sum. In our computations, we restrict the sum to pairs of type 1 particles that, at the time origin of each trajectory, are within a cutoff distance of $1.5\sigma_{11}$. Previous studies used the Lindemann index to locate phase boundaries in problematic cases, including finite [36] and quantum [37] systems. This index is well defined only when diffusion is strictly zero, and in this case it assumes a value (of the order of a few percent) that depends on T and $\hbar$ [38].

As soon as the diffusion sets in, the average distance between pairs of particles is no longer well defined, and the value of δ depends on the time span over which averages are computed. We exploit this qualitative difference in the time dependence of δ to magnify the effect of diffusion, and to analyze the mobility of our systems in phase space. In particular, we define a time-dependent version of the Lindemann index as

$$\delta(t)=\frac{1}{N_p}\sum_{i<j}\frac{\sqrt{\langle R_{ij}^2\rangle_t-\langle R_{ij}\rangle_t^2}}{\langle R_{ij}\rangle_t}, \tag{13}$$

where the variable t labeling $\langle R_{ij}^2\rangle_t$ and $\langle R_{ij}\rangle_t$ means that these averages are estimated over trajectories of length t. A plot of $\delta(t)$ for different values of T and $\hbar$ reveals three different behaviors (a representative example for $\hbar^2=1$ is shown in Fig. 4), analogous to those discussed in Sec. II and

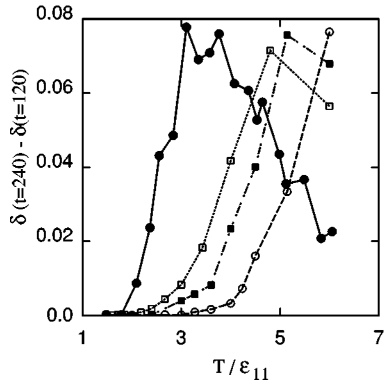

FIG. 5. Long time variation of the Lindemann index δ (see text) as a function of T. Filled circles, classical simulation ($\hbar^2=0$); empty squares, $\hbar^2=1/3$; filled squares, $\hbar^2=1/2$; empty circles, $\hbar^2=1$. The lines only provide a guide to the eye.

already observed in the classical simulations. At low temperature, where the system is solidlike, $\delta(t)$ converges quickly to its equilibrium value. At high temperature $\delta(t)$ grows steadily in time, with an apparent tendency to saturate to a limit close to 1/2. We also observe an intermediate range of temperatures in which $\delta(t)$ grows slowly by nearly discontinuous steps due to the jumplike motion of single particles or small clusters. We identify the first regime with a solidlike (glass) phase, and the other two with the fluid phase, discriminating further, on the basis of the diffusion mechanism, between a free flowing liquid at high T and a highly viscous liquid at intermediate T [39]. The boundaries between the different regimes can be easily located by computing the difference of $\delta(t)$ at two times t_1 and t_2, selected in such a way that at t_1 the index δ has already settled to its equilibrium value in the solidlike phase, while t_2 is significantly larger than t_1 (we choose, for instance, $t_1=120$ and $t_2=240$). By comparison with the full $\delta(t)$ curves, we then verify that $\delta(t_2)-\delta(t_1)$ is zero, to within the error bar ($\sim 4\times 10^{-4}$), in the solidlike phase, small but unambiguously greater than zero ($3\times 10^{-3}\leqslant \delta(t_2)-\delta(t_1)\leqslant 10^{-2}$) in the intermediate region, and fairly large ($\geqslant 10^{-2}$) in the liquidlike phase.

Since our analysis is based on the time dependence of δ, we have to rely on the approximate description of centroid mobility given by our MD simulations. However, the picture just described remains unchanged and unambiguous over a wide range of choices for t_1 and t_2 and, therefore, the conclusions do not depend crucially on the precise correspondence between simulation time and real time. In other words, the three different regimes can be interpreted in terms of the connectivity of the potential energy landscape as seen by particles at the typical energy set by the choice of T and $\hbar$: the system is locked into a single potential energy valley in the solidlike phase, it can migrate between valleys via activated jumps in an intermediate phase, and it can move continuously in the equilibrium liquid phase.

The results for $\hbar^2=0$, 1/3, 1/2, and 1 are displayed in Fig. 5. It is apparent that mobility decreases with increasing $\hbar^2$, rising our estimate for T_g from $T_g=2$ for the classical case ($\hbar^2=0$), to T_g=2.25, 2.66, and 3.25 for $\hbar^2=1/3$, 1/2, and 1, respectively. The determination of these temperatures is supported by detailed analysis of trajectories and of $\delta(t)$. Nonetheless, these values of T_g should be considered only as approximate, because of the several simplifications and assumptions made in connecting MD trajectories to real time diffusion. Moreover, we estimate the contribution to the uncertainty on T_g, due to statistical errors and discrete sampling of the temperatures around the glass point, to be $\Delta T_g \sim 0.1$

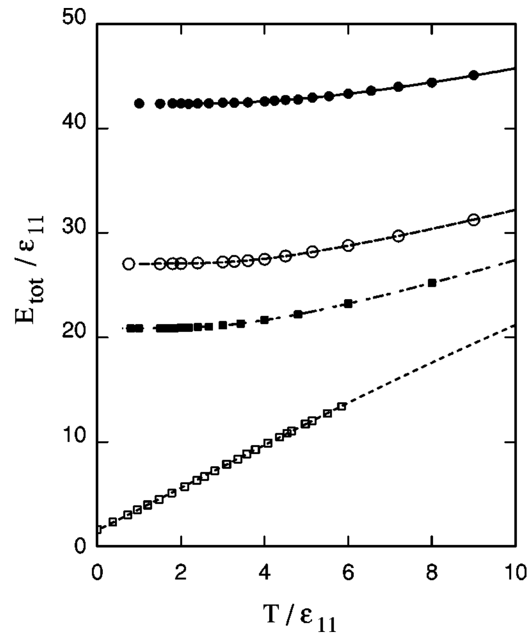

FIG. 6. Average total energy per particle E as a function of temperature. Filled circles, $\hbar^2=1$; empty circles, $\hbar^2=1/2$; filled squares, $\hbar^2=1/3$; empty squares, classical simulation $\hbar^2=0$.

Similar results, but with larger uncertainties [40], are obtained by computing the mean square displacement $\langle |R^C(t) - R^C(0)|^2\rangle$ for centroids.

We emphasize that the observed increase of T_g with increasing $\hbar$ depends on the anharmonic part of the model potential used in the present simulations, and there is no reason to expect that it is a general result. Moreover, the choice of the *NVT* ensemble for our simulations implies that, by changing $\hbar$, we are comparing systems at different values of pressure, which presumably increase with increasing $\hbar$ because of the enhancement of the zero point motion. This observation, together with the high sensitivity of T_g to pressure, suggests that performing the simulation in the *NPT* ensemble might provide qualitatively different results.

V. THERMAL PROPERTIES OF THE QUANTUM-MECHANICAL MODEL

As already anticipated, thermodynamic properties do not provide a sensitive probe of the glass transition for the quantum-mechanical systems considered in our simulations. This can be seen in Fig. 6, where the average total energy per particle E is reported as a function of T. The corresponding specific heat, computed by differentiating an orthogonal polynomial interpolation for $E(T)$, is shown in Fig. 7. A

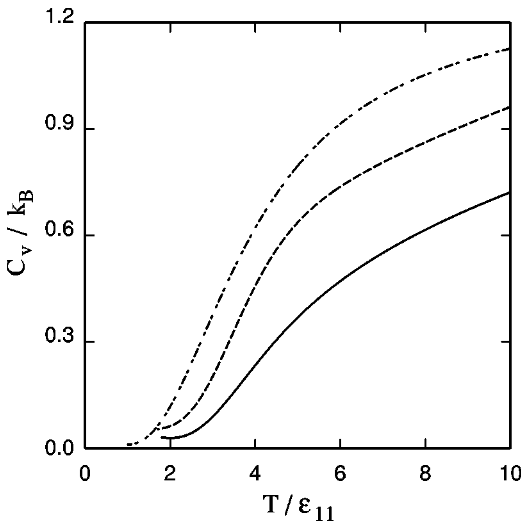

FIG. 7. Specific heat as a function of temperature for the quantum-mechanical systems. Full line, $\hbar^2=1$; dashed line, $\hbar^2=1/2$; dashed-dotted line, $\hbar^2=1/3$.

careful analysis of these curves, even guided by the determination of T_g obtained in Sec. IV, does not allow us to identify any anomaly that could be clearly attributed to the glass transition. Only a separate analysis of the kinetic (C_v^K) and potential energy (C_v^U) contributions to the constant volume specific heat C_v highlights a broad feature that could be related to the glass transition. In the classical case $C_v^K(T)$ is constant and the difference $C_v^U(T)-C_v^K(T)$ assumes exactly the same shape as C_v of Fig. 2(b). In the quantum case, as in the classical limit, this difference displays a broad peak (see Fig. 8) that could be considered analogous to the specific heat anomaly in Fig. 2(b). The peak moves continuously and monotonically towards higher temperatures with increasing $\hbar^2$, following the same qualitative trend as T_g. Provided that we disregard the secondary peaks of $C_v^U(T)-C_v^K(T)$ for $T \leqslant 2$, probably due to enhanced numerical noise in the fit, it becomes clear that the low T edge of the major peak corresponds well to our estimates of T_g based on the Lindemann ratio. The sensitivity of $C_v^U(T)-C_v^K(T)$ to T_g may be understood in terms of the particles localization corresponding to the glass transition, which causes a slight increase of the kinetic energy, and it occurs only when this effect is overcompensated by a corresponding drop in the potential energy.

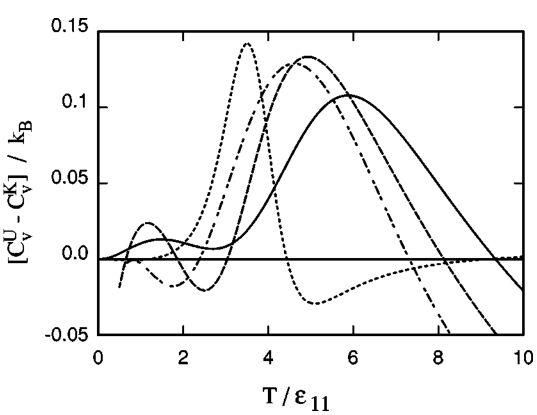

FIG. 8. Difference between the potential and the kinetic contributions to the constant volume specific heat as a function of temperature. Full line, $\hbar^2=1$; dashed line, $\hbar^2=1/2$; dashed-dotted line, $\hbar^2=1/3$; dotted line, $\hbar^2=0$ (classical limit).

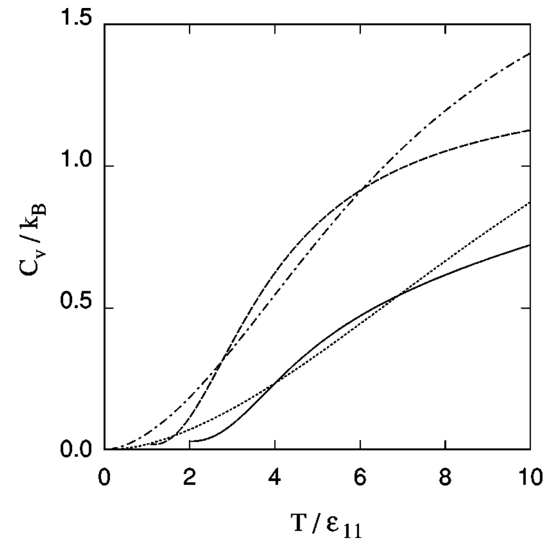

FIG. 9. Specific heat as a function of temperature, compared with its harmonic part, for two representative quantum systems. Full line, path-integral results for $\hbar^2=1$; dotted line, harmonic approximation for $\hbar^2=1$; dashed line, path-integral results for $\hbar^2=1/3$; dashed-dotted line, harmonic approximation for $\hbar^2=1/3$.

To investigate the relation of disorder, anharmonicity and thermodynamic properties, we select approximately 50 configurations, at random, from the quantum-mechanical trajectories at $T<T_g$, we minimize their potential energy with respect to the particle coordinates, and compute harmonic vibrational frequencies and eigenvectors. The structural and dynamical features characterizing the so obtained minima are discussed in the following sections, whereas here we focus on thermodynamic properties computed within the harmonic approximation. Although the minima are (at least slightly) different from each other from the structural point of view, they provide similar results for the thermodynamic properties, and therefore we choose to discuss the data concerning a single minimum for each value of $\hbar^2$, without averaging over different structures. Both the total energy and the specific heat computed in the harmonic approximation differ significantly from their PI counterparts, hence indicating the presence of strong anharmonic effects for these systems. In particular, for $\hbar^2=1/3$, 1/2, and 1, the total energy calculated within the harmonic approximation is significantly larger than the PI results over the entire temperature range covered by our simulations. The harmonic approximation overestimates the PI data also for C_v at low and high T, while the ordering is reversed at intermediate temperatures (see Fig. 9). The discrepancy at low T, in particular, could highlight an important link between quantum effects and anharmonicity. Zero point motion rises the energy of the particles well above the potential energy minimum, hence enhancing the effect of anharmonic terms already at low T. For our potential, this

apparently reduces the spectral weight of low-energy excitations, thus reducing the low temperature specific heat. The observed effect could also be interpreted in terms of the (expected) pressure increase with increasing $\hbar$, which is due to anharmonic effects. For instance, the bulk modulus of a LJ systems is known to increase sharply with increasing pressure [27] and this, in turn, rises the energy of the acoustic modes responsible for the low temperature specific heat.

The expected close relation between anharmonicity and disorder is demonstrated by a similar comparison of the specific heat for the monocomponent system described in Sec. III, which crystallizes during our quenches even in the quantum-mechanical cases. For these systems, the harmonic and PI estimates of the specific heat agree very well over a wide range of temperatures, and a Debye interpolation for the 2D phonons, resulting in

$$C_v(T)=4k_B\left(\frac{T}{\Theta_D}\right)^2\int_0^{\Theta_D/T}\frac{x^3e^x}{(e^x-1)^2}dx, \qquad (14)$$

where Θ_D is the Debye temperature, provides a very good fit of both for the values of $\hbar^2$ considered in our study.

For the two-component case, the Debye interpolation provides a far less accurate fit of the PI data. In all cases, because of the rather extreme choice of the values of $\hbar^2$, the best fit of the simulation data leads to very high values of Θ_D ($\Theta_D\sim30$ at $\hbar^2=1/3$, and $\Theta_D\sim50$ at $\hbar^2=1$ for the binary mixture, and the corresponding values for the monocomponent system are $\sim10\%$ higher). The increase of Θ_D with increasing $\hbar$, once again, is probably related to the increasing pressure due to anharmonicity and enhanced zero point motion, which stiffen acoustic waves in the system.

VI. STRUCTURAL PROPERTIES

For $\hbar^2=1/3$, 1/2, and 1, quantum delocalization broadens and smooths significantly the first three peaks of the radial distribution function $g(r)$ at all temperatures $T\leqslant 6$. As a result, the characteristic features in $g(r)$ (split second peak, a shoulder in the first peak, etc.) seen in the classical simulation at low T, and often associated with the glass transition, are lost for the quantum systems. Moreover, as expected, the already moderate temperature dependence of the glassy $g(r)$ is further reduced by the zero point motion, which makes $g(r)$ nearly independent of T and liquidlike over an extended range of conditions. Both effects contribute to render the glass transition practically undetectable on the basis of structural properties alone, at least for the choice of parameters used in our simulations. These results are illustrated in Fig. 10, which shows the radial distribution function $g_{11}(r)$ for type 1 particles [41], computed at $T=2$ and $T=6$, for the classical case ($\hbar^2=0$) and for two quantum samples ($\hbar^2=1/3$ and $\hbar^2=1$). The qualitative features apparent in this figure are reflected in similar trends for the structure factor $S(k)$, whose peaks are also broadened and smoothed in going from the classical to the quantum cases.

Despite the major broadening and the loss of characteristic features in $g(r)$ and $S(k)$, a detailed analysis of simulation snapshots shows that the major role of quantum effects is to superimpose a low-T fuzziness to particle configurations that are, to a large extent, equivalent to the classical ones. This is verified again by selecting configurations from either classical or quantum trajectories, and minimizing their potential energy by quenched MD. The underlying minimum energy geometries determined in this way are all qualitatively similar, with only small quantitative differences discussed in Sec. VII. The radial distribution functions relative to the minimum energy structures originated from quantum trajectories are indistinguishable from their classical (quenched) counterparts and, in particular, they all display the characteristic features of glasses. Moreover, the average size and shape of type 1 microcrystals and type 2 elongated islands are the same in the classical and quantum cases.

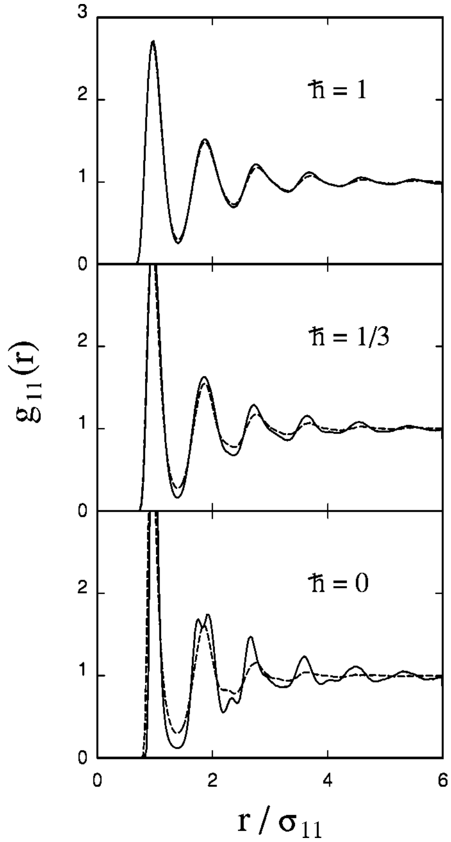

FIG. 10. Radial distribution function $g_{11}(r)$ for type 1 particles computed at three different values of $\hbar$. Full line, $T=2$; dashed line, $T=6$.

Unfortunately, the emergence of glassy features in the radial distribution function of the quenched quantum configurations cannot be used to determine T_g because similar geometries and $g(r)$ or $S(k)$ are obtained by quenching configurations from temperatures above T_g.

A different strategy for identifying structural signatures of T_g is suggested by the close relation between the glass transition and the phase space mobility of path centroids discussed in Sec. IV. We verify that, for quantum samples, the radial distribution function of centroids (a quantity that is readily available in simulation, but not in experiments) undergoes the characteristic structural changes associated with the glass transition at temperatures that correspond well to the T_g estimated in Sec. IV for the same values of $\hbar^2$. These changes, however, take place less suddenly than the change in the time dependence of the Lindemann ratio, and the corresponding determination of T_g is affected by larger uncertainties. The analysis of the centroid radial distribution functions, therefore, provides only a secondary diagnostic tool that can be used to verify values of T_g determined with more accurate methods.

VII. LOW-ENERGY LOCALIZED EXCITATIONS AND TUNNELING CENTERS

Low-energy excitations represent one of the most characteristic properties of glasses, giving rise to equally universal features in their specific heat. At temperatures of ~ 10 K, a characteristic peak in the temperature dependence of the specific heat (the so-called Boson peak) is attributed to soft quasilocalized harmonic vibrations. At very low temperatures ($T \sim 1$ K) the specific heat of glasses displays an anomalous linear dependence on temperature, which is associated to tunneling centers (two-level systems, TLS) [42]. It is generally accepted that these two types of excitations are closely connected, and this point of view is the basis for the so-called soft potential model [43], which provides a unified description of both the low (~ 10 K) and very low (~ 1 K) temperature universal properties of glasses.

Computer simulation has already been used to identify TLS in amorphous samples produced by classical MD or MC [8–11]. For a variety of simple model potentials, the TLS found by simulation appear to be due to the oscillation of localized clusters (containing up to 20–50 particles) between local energy minima that are almost degenerate and close in space.

Despite these recent major advances in our understanding and visualization of TLS, several features of these centers are still unknown. A basic unsolved issue, for instance, concerns the relative role of quantum tunneling and thermal oscillations in TLS.

In our simulations the evolution between the configurations in which our system is found is due both to thermal and quantum fluctuations. The thermal fluctuations are reflected mainly in the real-time evolution of the system, while quantum fluctuations give rise to structural changes among different imaginary-time slices at the same real time. Therefore, we can decouple these two effects, to an extent, by comparing configurations at different imaginary times (i.e., different j) but same real time, or different real time but same imaginary time.

In our simulations, we identify tunneling centers by quenching configurations separated by regular real (every 12τ) *or* imaginary (at $\tilde{t}=0$ and $\tilde{t}=\beta/2$) time intervals, along trajectories at temperatures $T<T_g$ so that diffusion is negligible. We discuss, in particular, the results for $\hbar^2=1$, obtained by analyzing trajectories at $T=1$ and $T=1.5$. All quenches produce energy minima that differ by at least a few details in the system configuration. In most cases, the difference is due to a few (~ 10) isolated particles located at the boundary between microcrystals of type 1 particles and type 2 elongated clusters. For different minima, the position of each of these particles changes by an amount of the order of σ_{11}, i.e., well outside the uncertainties due to the energy minimization routine. However, the energy difference among these minima is very small ($\Delta E \leqslant 0.01$), and also the barrier ($E_B \sim 0.02$–0.03) is two orders of magnitude lower than both the zero point energy of our particles at $\hbar^2=1$ and the (classical) thermal energy at T_g. Therefore, we do not consider these minima as belonging to tunneling centers, rather we associate all of them to a unique broad energy basin.

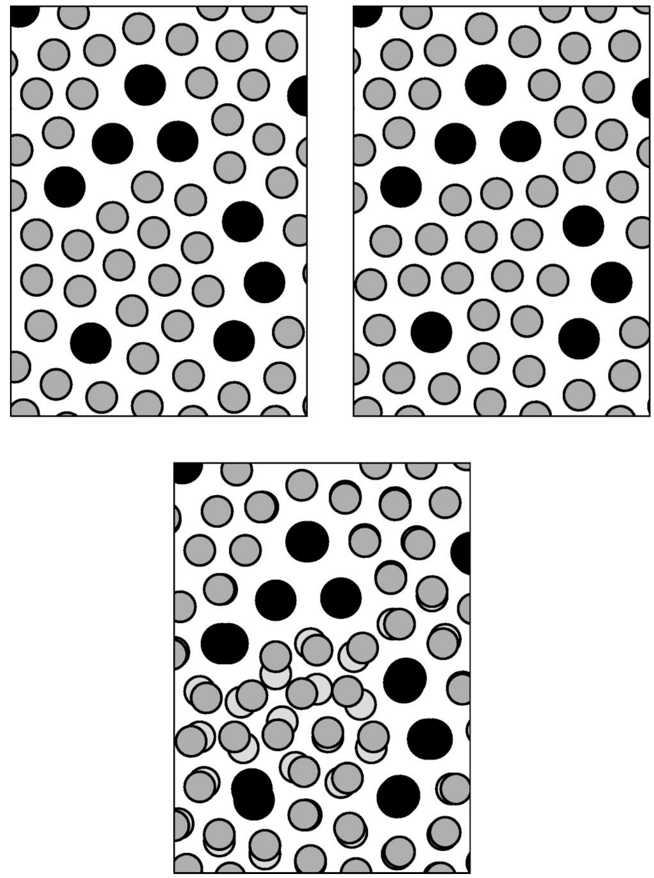

FIG. 11. Upper panels: same portion of the system geometries corresponding to potential energy minima found by quenching configurations at the same MD time and separated by $\beta/2$ in imaginary time. Bottom panel: superposition of the two panels above. The original configurations have been selected on a trajectory at $T=1$ and $\hbar^2=1$. Gray and black circles represent the particles of type 1 and 2, respectively.

More interesting are pairs of energy minima that differ in the position of a localized cluster made of ~ 15–20 particles. These energy minima are still nearly degenerate, but the potential energy barrier separating them is no longer negligible ($E_B \sim 0.1 T_g$). The majority of these pairs (see Fig. 11 for a representative example) result repeatedly from quenches of configurations at the same real time and different imaginary times. We attribute the observed oscillations within these pairs to quantum tunneling. A few additional pairs are found by quenching configurations separated by 12τ in real time but at equal imaginary time. We attribute the observed crossing between these pairs to thermal oscillations.

As expected, the identification of single events as

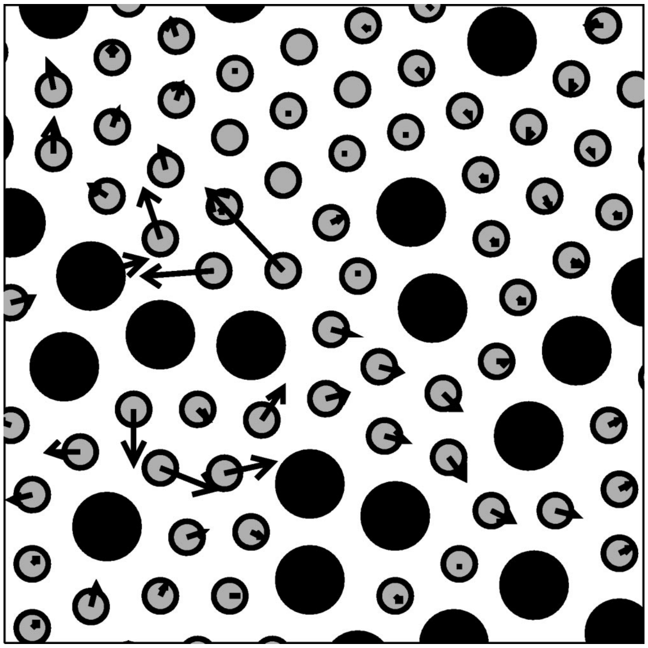

FIG. 12. Particle displacement (represented by the arrows) for a soft quasilocalized mode belonging to the vibrational spectrum of one of the minima in Fig. 11. Gray and black circles represent the particles of type 1 and 2, respectively.

quantum-mechanical tunneling events or as thermal oscillations is not completely unambiguous, since at any $T>0$ quantum and thermal fluctuations are necessarily both present. Therefore, even for the events that we identify as thermal, the isomerization does not take place exactly at the same real time for every imaginary time slice, and, conversely, quantum events require a short but nonvanishing real time to take place. The distinction, therefore, relies mainly on the different time scale for the transformation in real and imaginary time: thermal events occur for all the imaginary-time slices within a few simulation steps, while quantum tunneling is identified by structural differences among different imaginary-time slices that persist for long simulation times. More extensive simulations are underway to provide a statistically significant classification of energy minima pairs for a wider range of temperatures and $\hbar^2$.

The localized clusters involved in either the quantum tunneling or the thermal oscillations are similar in size, shape and location (at microcrystal boundaries) to those supporting the low-energy quasilocalized modes found by harmonic analysis for the classical samples (see Sec. III). It is important to remark, however, that the clusters identified by PI simulation and by harmonic analysis are *not* the same. We verify this point by computing the harmonic frequencies and eigenvectors for each of the minima found in the tunneling analysis. We find that each of the harmonic spectra contains at least a few low-energy quasilocalized modes (illustrated in Fig. 12) completely analogous to those found in the classical case. However, in all cases, the particles that participate significantly in the tunneling process are not those showing a significant displacement in the quasilocalized harmonic modes. This difference underlines the (expected) major role of anharmonic effects in the low-energy dynamics of our

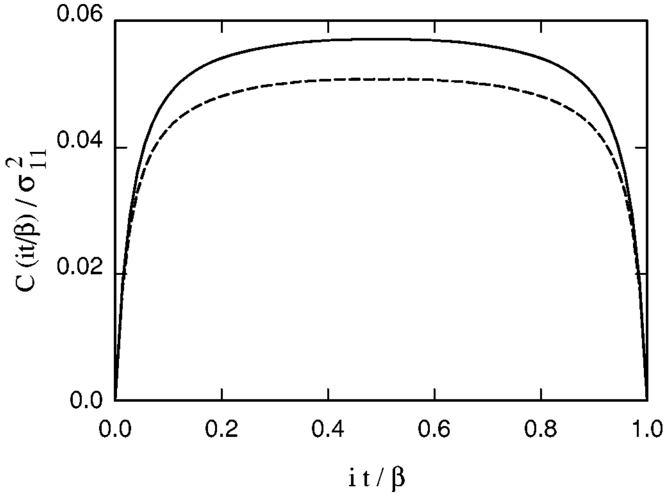

FIG. 13. Imaginary-time correlation function for type 1 (full line) and type 2 (dashed line) particles for a system at $T=1$ and corresponding to $\hbar^2=1$.

quantum systems, for which the zero point motion rises the energy of the system well above the potential energy minima visited by the system at low T.

In our case, the imaginary-time correlation functions [such as $C(\tilde{t})=(1/N)\langle\Sigma_i|r_i(\tilde{t})-r_i(0)|^2\rangle$], often used in PI studies to characterize thermal and dynamical properties of quantum systems (see Ref. [20]), do not provide new information relevant for the glass transition. At all temperatures, for instance, $C(\tilde{t})$ displays the usual shape (see Fig. 13) typical of systems with strong anharmonic effects or with disorder induced localization. With increasing T, the amplitudes of quantum fluctuations are, as expected, progressively reduced. A plot of $C(\tilde{t}=i\beta/2)$ as a function of T (see Fig. 14) displays a change in slope at a temperature $T\sim4.5$ (significantly higher than T_g) which, for our systems, corre-

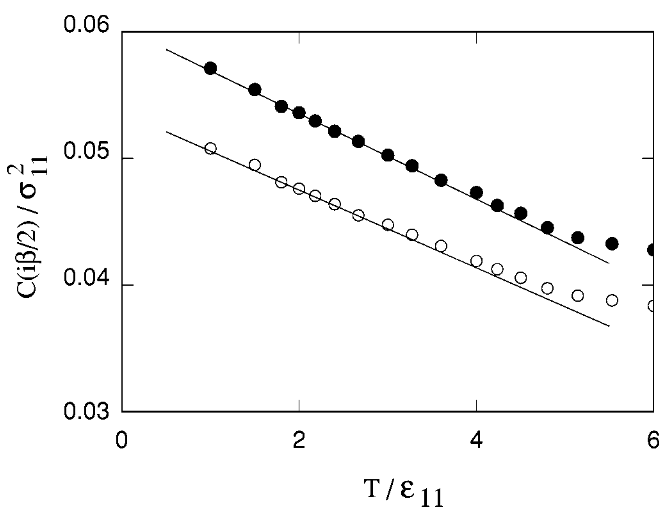

FIG. 14. Temperature dependence of the imaginary-time correlation function $C(\tilde{t})$ at imaginary time $\tilde{t}=i\beta/2$ for type 1 (filled circles) and type 2 (empty circles) particles in a system at $T=1$ and corresponding to $\hbar^2=1$. The lines refer to linear fits of the data for $T\leq2$, and have been added to provide a guide to the eye.

sponds to the change from jumplike mobility to liquidlike diffusion. More systematic studies using different potentials are required to verify whether this correlation has a general validity.

VIII. SUMMARY AND CONCLUDING REMARKS

The glass transition in a quantum-mechanical LJ mixture in two dimensions has been investigated by path-integral MD simulations. All particles have mass equal to one, they are assumed to be distinguishable, and the strength of quantum effects is measured by the parameter $\hbar^2$ that, in our study, takes the values 0 (the classical limit), 1/3, 1/2, and 1. For all simulations, T is initially set to a high value, so that the system clearly is in the liquid state, and then progressively decreased until nearly zero. The analysis of configurations, diffusion coefficient, and thermal and structural properties (i.e., radial distribution function and structure factor) shows that the classical sample undergoes a glass transition at $T_g=2$. The determination of T_g for the quantum-mechanical samples is far more difficult. The path-integral scheme provides only imaginary-time correlation functions, whose analytic continuation to real time, required to compute dynamical coefficient, is known to be severely ill conditioned [44]. Concerning the thermodynamic properties, quantum delocalization and zero point energy prevent the appearance of the diagnostic features that, in classical systems, identify the glass point. We rely instead on the analysis of phase space mobility for path centroids that, with decreasing temperature, reveals three different regimes: (i) a fast and continuous flow at high T; (ii) discrete jumps at intermediate temperatures, and (iii) localized oscillations at low T. We interpret these regimes in terms of connectivity of the potential energy valleys visited by the system, and we associate the first regime with a liquid at equilibrium, the second with a sluggish liquid state, and the third with a solidlike glass phase. The temperature separation of the three phases depends only very weakly on the time scale of the observation, and therefore we identify the glass transition with the transition between the last two regimes. The estimated T_g is 2, 2.25, 2.66, and 3.25 for $\hbar^2=0$, 1/3, 1/2, and 1, respectively, i.e., T_g increases monotonically with $\hbar$. This trend is due to the dominant anharmonic contributions of our potential model, and could be different for other types of interparticle interactions. Moreover, the sensitivity of T_g to pressure suggests that the results could be quantitatively and even qualitatively different by simulating the glass transition in the *NPT* ensemble rather than in the *NVT* ensemble adopted in our study. Nevertheless, the analysis of centroid trajectories discussed above would still provide a method to determine T_g.

The close connection between path centroid dynamics and glass transition is reflected in the fact that the radial distribution function and structure factor *for centroids* (both easily computed in simulations, but not measured in experiments) develop additional features at T_g. For quantum systems, therefore, structural functions of the centroids play the same role as $g(r)$ and $S(k)$ of particles in classical systems. The determination of T_g via the centroids structural features, however, is less accurate than the estimate via the phase space mobility because structural changes develop more gradually over a temperature interval of width $\Delta T\sim 0.5$.

The identification of T_g allows us to relate the glass transition to an excess in the potential energy contribution to C_v with respect to the corresponding kinetic energy part. This anomaly can be interpreted in terms of the interplay between the kinetic energy cost and the potential energy gain due to the localization of the particles at T_g. In this respect, quantum systems differ significantly from classical systems, for which the only two quantities competing at the glass point are the potential energy and the entropy.

The particle dynamics in the glass phase has been investigated by identifying the different minima in the potential energy surface visited by the system at $T<T_g$. We observe oscillations between degenerate pairs of minima, which differ in the configuration of localized clusters made of $\sim$15–20 particles. The crossing between different minima occurs predominantly as a function of imaginary time at fixed real (MD) time. We interpret these oscillations as quantum tunneling. In a few cases, we observe thermally activated oscillations between minima occurring nearly simultaneously for all the P imaginary time replicas of the system.

The harmonic spectrum for each of the potential energy minima identified from either classical or quantum trajectories contains a few ($\sim$5–10) soft quasilocalized modes, which involve clusters of particles very similar to those giving rise to the thermal or quantum oscillations described above. However, we verified that the clusters involved in these soft quasilocalized harmonic modes are different from those causing tunneling. This difference is somewhat unexpected since, in classical systems, soft quasilocalized modes and thermal tunneling centers usually involve the same groups of particles. This different behavior can be understood in terms of the high zero point energy of our systems (partly due to their high density), which rises the energy of the particles well beyond the potential energy minima and amplifies anharmonic effects. Consequently, the harmonic analysis in the characterization of the low T dynamics of quantum systems becomes less relevant.

The identification of tunneling centers and the analysis of their quantum versus thermal character, together with the determination of the glass transition temperature T_g for quantum systems, are the major results of our study. We stress that, in order to amplify all the differences with respect to the classical picture, we selected parameters corresponding to strong quantum effects. Further computations with different parameters and different potentials [45] are required to simulate more realistic models of glasses that can be compared with experimental results.

ACKNOWLEDGMENTS

The work presented in this paper began when both of us were at the Institut für Festkörperforschung (IFF), Forschungszentrum Jülich, Germany. We thank Dr. R. H. Schober for a critical reading of the manuscript, and for making us aware of several important papers and previous findings related to this work.

[1] P.G. Debenedetti and F.H. Stillinger, Nature (London) **410**, 259 (2001).

[2] See, for instance, T. Odagaki, Y. Hiwatari, and J. Matsui, in Dynamics of Glass Transition and Related Topics, Proceedings of the 7th Yukawa International Seminar, edited by T. Odagaki, Y. Hiwatari, and J. Matsui [Prog. Theor. Phys. Suppl. **126**, R1 (1997)].

[3] See, for instance, B. Coluzzi, G. Parisi, and P. Verrocchio, Phys. Rev. Lett. **84**, 306 (2000), and references therein.

[4] The terms *glass* and *amorphous* are used here as equivalent, although a distinction is made by some authors.

[5] A. Heuer and R. Silbey, Phys. Rev. B **53**, 609 (1996).

[6] B.B. Laird and H.R. Schober, Phys. Rev. Lett. **66**, 636 (1991); H.R. Schober, and B.B. Laird, Phys. Rev. B **44**, 6746 (1991).

[7] S.D. Bembenek and B.B. Laird, Phys. Rev. Lett. **74**, 936 (1995).

[8] G. Daldoss, O. Pilla, G. Viliani, C. Brangian, and G. Ruocco, Phys. Rev. B **60**, 3200 (1999).

[9] C. Brangian, O. Pilla, and G. Viliani, Philos. Mag. B **79**, 1971 (1999).

[10] D. Dab, A. Heuer, and R.J. Silbey, J. Lumin. **64**, 95 (1995).

[11] A. Heuer and R.J. Silbey, Phys. Rev. Lett. **70**, 3911 (1993).

[12] In most of our simulations, however, quantum effects are still less pronounced than in several simulation studies devoted to helium close to the superfluid transition. See Ref. [21] for a review.

[13] J.-P. Hansen in *Computer Simulation in Materials Science*, Vol. 205 of *NATO Advanced Studies Institute, Series E: Applied Sciences*, edited by M. Meyer and V. Pontikis (Kluwer, Dordrecht, 1991).

[14] For a discussion of this so-called inherent structure see, for instance, F.H. Stillinger and T.A. Weber, Phys. Rev. A **25**, 978 (1982).

[15] See, for instance, G. Weiss, K. Eschenröder, J. Classen, and S. Hunklinger, J. Low Temp. Phys. **111**, 321 (1998).

[16] The LJ potential is matched to a cubic polynomial at $r=3.5\sigma_{22}$ in order to have a potential that vanishes beyond $r=4\sigma_{22}$, and is everywhere continuous with its first derivative.

[17] G. Johnson *et al.*, Phys. Rev. E **57**, 5707 (1998).

[18] Y.J. Wong and G.V. Chester, Phys. Rev. B **35**, 3506 (1987).

[19] R.P. Feynman and A.R. Hibbs, *Quantum Mechanics and Path Integrals* (McGraw-Hill, New York, 1965).

[20] D. Chandler, in *Theory of Quantum Processes in Liquids*, Proceedings of the Les Houches Summer School, Session 51, edited by D. Levesque, J.-P. Hansen, and J. Zinn-Justin, Liquids Freezing and Glass Transition, Part 1 (Elsevier, Amsterdam, 1991), p. 193.

[21] D.M. Ceperley, Rev. Mod. Phys. **67**, 279 (1995).

[22] Because of possible ergodicity problems at high values of P, Monte Carlo simulations have been performed to verify that the results are insensitive to the simulation method used to sample the phase space. The Monte Carlo implementation included both single-bead moves and collective moves, displacing either an entire *real* particle (i. e., P connected beads), or a segment of the harmonic chain representing one particle. The results are equal to those provided by MD to within the error bar.

[23] M.P. Allen and D.J. Tildesly, *Computer Simulation of Liquids* (Clarendon, Oxford, 1989).

[24] For $\hbar^2=1$ and $T=1$, for instance, if we increase the value of P by 50% with respect to the prescription of Eq. (4), (i.e., from $P=72$ to $P=108$), the total energy E_{tot} increases by 2.4%. Moreover, the change in the total energy differences, which are much more important than E_{tot} itself for the determination of structural and dynamical properties, is significantly smaller than the change in E_{tot}.

[25] M.F. Herman, E.J. Bruskin, and B.J. Berne, J. Chem. Phys. **76**, 5150 (1982).

[26] Reference [21] contains an explicit derivation of the virial estimator that takes into account corrections due to periodic boundary conditions (pbc). However, in our case the particles do not exchange (they are distinguishable), and single particles paths extend over very short distances. Therefore, they never cross the boundaries of the simulation box. As a result, the correction due to pbc is identically zero.

[27] Alternative strategies to improve the accuracy of kinetic energy estimators are discussed in P. Schöffel and M.H. Müser, Phys. Rev. B **63**, 224108 (2001).

[28] The velocity of all particles is set to zero whenever the $2N$-dimensional scalar product of velocities and forces becomes negative.

[29] J. Cao and G.A. Voth, J. Chem. Phys. **100**, 5093 (1994).

[30] G.A. Voth, in *Advances in Chemical Physics*, edited by I. Prigogine and S. A. Rice (Wiley, New York, 1996), Vol. XCIII.

[31] See, for instance, R. Car and M. Parrinello, Phys. Rev. Lett. **55**, 2471 (1985).

[32] With a different choice of units, defined by $\hbar=\epsilon_{11}=\sigma_{11}=1$, the three cases analyzed correspond to $M=3$, 2, and 1. We prefer the set of units specified in Sec. II because having an equal mass in all cases allows us to use the same unit of time and the same time step for all simulations.

[33] Our choice for the equivalent monocomponent system differs from the more common relation: $\sigma^2=x_1^2\sigma_{11}^2+2x_1x_2\sigma_{12}^2+x_2^2\sigma_{22}^2$, and corresponds to the definition given in D.N. Perera and P. Harrowell, Phys. Rev. E **59**, 5721 (1999).

[34] The participation ratio pr for the ith eigenmode of frequency ω_i is defined as $pr(\omega_i)=\{N[\Sigma_j|\mathbf{B}_i^j(\omega_i)|^2]^2\}/\Sigma_j|\mathbf{B}_i^j(\omega_i)|^4$, where the sum is over all particles, and $\mathbf{B}_i^j$ is the displacement of particle j for the ith harmonic mode. See, for instance, R.J. Bell, P. Dean, and D.C. Hibbins-Butler, J. Phys. C **3**, 2111 (1970); W.M. Wisscher, J. Non-Cryst. Solids **8**-**10**, 477 (1972).

[35] More precisely, these modes are quasilocalized, since they are hybridized with a broad band of delocalized modes. See the discussion in Ref. [43] for further details.

[36] For recent application see: A. Proykova, S. Pisov, and R.S. Berry, J. Chem. Phys. **115**, 8583 (2001).

[37] C. Chakravarty, Phys. Rev. B **59**, 3590 (1999).

[38] For classical systems $\delta\sim 10\%$ is the well known limit of stability for crystals introduced by Lindemann. For quantum systems the critical δ is less well established, but somewhat larger than in the classical case, see H. Xu, J.-P. Hansen, and D. Chandler, Europhys. Lett. **26**, 419 (1994).

[39] The discrete jumps seen in the intermediate regime of our simulations cannot be attributed to the residual diffusion that occurs even in glasses. A rough estimate of their real-time frequency, using values for $\sigma\approx 2$ Å $\epsilon\approx 100$ K, and $M\approx 20$ atomic mass units, shows that the corresponding diffusion coefficient ($D\approx 10^{-8}$ cm^2/s) is still in the (viscous) liquid range.

[40] The computational advantage of the Lindemann ratio with respect to the diffusion coefficient is due to the additional averaging over particle pairs that reduces fluctuations.

[41] In Fig. 10 we report $g_{11}(r)$ instead of the total radial distribution function $g(r)=x_1^2 g_{11}(r)+2x_1x_2g_{12}(r)+x_2^2g_{22}(r)$ because the structure of $g(r)$ is complicated by the superposition of peaks originated by the three different components g_{11}, g_{12}, and g_{22}.

[42] P.W. Anderson, B.I. Halperin, and C.M. Varma, Philos. Mag. **25**, 1 (1972); W.A. Phillips, J. Low Temp. Phys. **7**, 351 (1972).

[43] V.G. Karpov, M.I. Klinger and F.N. Ignatiev, Zh. Eksp. Teor. Fiz **84**, 760 (1983) [Sov. Phys. JETP **57**, 439 (1983)]; U. Buchenau *et al.*, Phys. Rev. B **43**, 5039 (1991); V.L. Gurevich, D.A. Parshin, J. Pelous, and H.R. Schober, *ibid.* **48**, 16 318 (1993).

[44] See, for instance, M. Jarrel, and J.E. Gubernatis, Phys. Rep. **296**, 133 (1996).

[45] A path-integral simulation for the prototype glass former, i.e., SiO_2 has been recently reported by Chr. Rickwardt, P. Nielaba, M.H. Müser, and K. Binder, Phys. Rev. B **63**, 045204 (2001); this study, however, is focused on thermodynamic properties, and does not address the determination of the glass transition that, for SiO_2, takes place at temperatures for which quantum effects are not very important.